Journal of Inorganic and Organometallic Polymers and Materials (2018) 28:1235–1245
https://doi.org/10.1007/s10904-018-0836-5

Methacrylate Functionalized MWCNTs/PDMS-Polyurethane Methacrylate UV-Curable Nanocomposites

Kübra İlgün[1] · Burcu Oktay[1] · Nilhan Kayaman Apohan[1]

Received: 16 November 2017 / Accepted: 22 March 2018 / Published online: 28 March 2018

Abstract
Polyurethane (PU)-carbon nanotube composites have gained interest in the area of aerospace, automobiles, fuel cells electrical appliances and communication related applications. However, there is still insufficient information on PU-carbon nanotube composites. In this study, hydrophobic and high performance UV-curable nanocomposites were prepared by using surface functionalized multi-walled carbon nanotubes (MWCNT). First, MWCNT were treated with acid solution (HNO_3/H_2SO_4) and then grafted with poly(ethylene glycol) methacrylate (PEGMA) to introduce UV-photopolymerization sites. Different amounts of methacrylate tethered MWCNT and sol–gel precursor or hydrophobic nanosilica were added to PDMS—polyurethane methacrylate based UV-curable formulation and cured by UV irradiation. The composites were also thermally treated (post-cure). The effects of the carbon nanotube, the sol–gel precursor and the hydrophobic nanosilica content on thermal, mechanical and morphological properties of the nanocomposite films were investigated. The addition of the sol–gel precursor and hydrophobic nanosilica increased thermal stability with regard to the base formulation. The addition of MWCNT and silica increased the modulus of the composite from 245 to 318 MPa with regard to the base formulation. Moreover, the thermal decomposition range was increased with addition of the modified MWCNTs. The morphology of the composite films was also carried out by using scanning electron microscopy (SEM). Morphological investigations showed that better dispersion of nanoparticles and performance were achieved when the surface functionalized MWCNTs and hydrophobic silica nanoparticles used together in nanocomposite preparation.

Keywords Carbon nanotube · Surface functionalization · UV curing · Nanocomposite

1 Introduction

Carbon nanotubes (CNTs) have been considered as nanofiller in field of nanomaterials because of their notable many advantages other carbon nanomaterials [1]. They are used for wide range of applications such as thermal interface materials, energy storage and filtration applications [2]. sp2 carbon–carbon bonds of CNTs are stronger than the sp3 bonds. This bonding makes the structure of CNT extremely strong that effects the thermal and mechanical properties [3]. The incorporation of CNTs into polymer matrix has been limited because of the effective dispersion problem of its. The strong van der Waals force and π–π stacking occur along the long tube that causes aggregation [4]. The problem can be overcome by enhancement of poor interfacial interaction between CNTs and polymer matrix.

CNTs can be effectively integrated to the polymer by modification of their organic constituents. The structure and originality of CNTs are not altered but further functionalization of CNTs is achieved [5]. Non-covalent and covalent modifications have been made on the surface of CNTs [6]. The sidewalls of the tubes can be covalently functionalized with reaction of high reactivity chemical molecules such as fluorine. Another method is defect functionalization, which creates defect sites on both the sidewalls and end tips of CNTs by an oxidation reaction with HNO_3, H_2SO_4 or a mixture of them [7]. The defect sites can be modified by bonding with –COOH or –OH groups. These functional groups allow to further chemical reaction of CNT for a later stage. For example, the carboxyl groups can react with acryl chloride groups. In addition, the carboxyl groups allow the decoration of CNTs with various

✉ Nilhan Kayaman Apohan
napohan@marmara.edu.tr

[1] Department of Chemistry, Marmara University, 34722 Goztepe-Istanbul, Turkey

functional groups by esterification, amidation, silanation, polymer grafting, thiolation, alkylation and arylation [8].

The hydrophilicity of CNTs can be changed with attachment of the polar groups. Therefore CNTs can form strong particle-polymer interactions with many polymers. Polymer–CNT nanocomposites possess high mechanical and functional properties with respect to neat CNTs [9, 10]. Since the preparation of a polymer–CNT composite was first reported in 1994, they have been successfully prepared from solution blended, melt blended, and in-situ polymerized CNT/polymer mixtures. But in these methods, removal of solvent can be required [11, 12]. Another method is in-situ photopolymerization that viscosity can be easily controlled and thus the dispersion of CNTs gets easy [13]. Extensive studies have been carried out producing CNT/polymer composites by irradiation of UV-light. Zhou et al. investigated the compatibility of multi-wall carbon nanotube with hyperbranched polymer matrixes. CNT was chemically bonded with the UV curable matrix by crosslinking photopolymerization. According to the results, the mechanical properties of the MWCNT/polymer films greatly improved [14]. Eitan et al. synthesized carboxylated-MWCNTs further reactions with di-glycidyl ether of bisphenol-A-based epoxide resin [15]. Fan and coworkers prepared polystyrene-grafted multiwalled carbon nanotubes. Moreover, the prepared product used to initiate the polymerization of 4-vinylpyridine to get polystyrene-*b*-poly(4-vinylpyridine)-grafted multiwalled carbon nanotubes [16]. There is currently insufficient information on polyurethane (PU)-carbon nanotube composites systems. However, the limited literature information clearly indicates that advantages of PU-CNT composites over traditional PU systems [17]. For examples, the fatigue life of MWCNT-PU composite used for wind blades is higher compare to neat PU [18]. It is seen that the glass transition temperatures of neat PU and PU-MWCNT composite have dramatic differences from each other [19]. The large number of reports indicated that the addition of CNTs to polyurethanes, the tensile strength, modulus, thermal stability and electrical conductivity increased [20].

The main objective of this study is to prepare and characterize hydrophobic and high performance UV-cured MWCNT bearing polyurethane based composite films. PDMS-polyurethane methacrylate resin was synthesized from PDMS, IPDI and HEMA. MWCNT was functionalized with PEGMA. After UV curing of surface functionalized MWCNTs containing UV curable formulation, the composite films were thermally treated to promote crosslinking. Moreover, the effect of nanosilica addition on morphological properties, and other characteristic properties such as thermal stability, mechanical strength was investigated. The contact angles of the polymeric films were also measured to assess surface wettability.

2 Experimental

2.1 Materials

The aliphatic polyester acrylate (LAROMER LR 8992) and 1-hydroxy cyclohexyl phenyl ketone (Irgacure-184) were generously provided by BASF Turkey. Carbon nanotube (multi-walled, purity 95%, diameter = 10–15 nm, length = 0.1–10 µm, density = 1.7–2.1 g/cm^3) was purchased by Alfa Aesar. Hydroxyl-terminated PDMS (MW = 2080 g/mol, hydroxyl content 40 mg/KOH, Aldrich), 2-hydroxyethyl methacrylate (HEMA) (Merck), 3-methacryloxypropyltrimethoxysilane (MPTMS) (3-methacryloxypropyltrimethoxysilane), isophorone diisocyanate (IPDI) (Fluka) and tetraethyl orthosilicate (TEOS) (Aldrich) were used. Dibutyl tin dilaurate (DBTDL) (Henkel) was used as a catalyst. 4-(Dimethylamino)pyridine (DMAP) and dicyclohexylcarbodiimide (DCC) were obtained from Aldrich.

2.2 Synthesis of Poly(Dimethyl Siloxane-Urethane Methacrylate)

Poly(dimethyl siloxane-urethane methacrylate) (PDMS-U methacrylate) was synthesized according to our previous work [21]. Hydroxyl-terminated PDMS (Aldrich) was dried under vacuum at 40 °C before used. The all equipment was kept for 24 h at 120 °C. 12.75 g (0.055 mmol) IPDI was charged into three-necked flask equipped with a mechanical stirrer and thermometer under a nitrogen atmosphere. 7.3 g (0.055 mmol) of HEMA was added to the flask using a pressure-equalizing dropping funnel to the vigorously stirred IPDI in 30 min. Then, the mixture was further stirred for 1 h at room temperature. The reaction system was heated to 75 °C and kept. 58.5 g (0.0275 mmol) hydroxyl terminated PDMS was slowly introduced during 30 min. 5 µL of DBTDL was added to the reaction mixture as catalyst. The reaction was stirred for 5 h. The reaction pathway is shown in Scheme 1. The characteristic –NCO band disappeared at the end of the reaction. The product was identified by ATR–FTIR.

2.3 Synthesis of Methacrylate Tethered Multi-walled Carbon Nanotube

The functionalization of MWCNTs is as follows: firstly oxidation of CNTs was carried out in acidic medium. 1 g of MWCNT was dispersed in a solution of 100 mL sulfuric acid/nitric acid mixture (3/1 v/v) and stirred for 2 h at 50 °C. The suspension was refluxed at 120 °C for 4 h. The product was washed with deionized water and acetone until

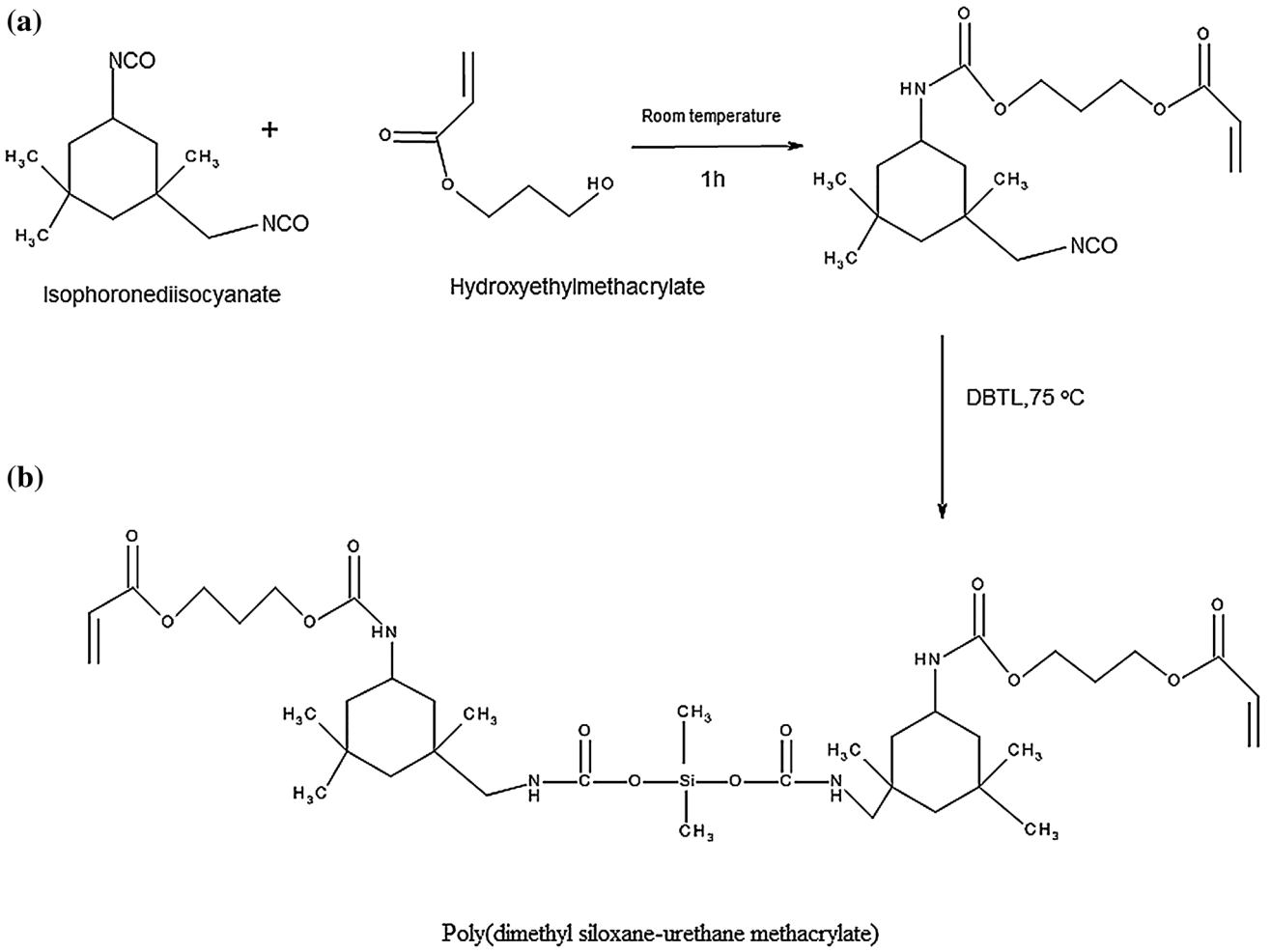

Scheme 1 **a** IPDI with two HEMA derivative and **b** IPDI with one HEMA derivative and synthesis of poly(dimethyl siloxane-urethane methacrylate)

pH neutral and then it was separated by a centrifugation and drying in a vacuum oven at 50 °C.

After the oxidation reaction in acidic solution, PEGMA incorporated to MWCNTs. 1 g of oxidized-MWCNTs are dispersed in 50 mL of anhydrous dichloromethane via ultrasonication for 30 min. 1.1 g (0.009 mol) of 4-(dimethylamino)pyridine (DMAP) and 2.68 g (0.013 mol) of dicyclohexylcarbodiimide (DCC) were added and stirred for 2 h. 14 g (0.028 mol) of PEGMA was added to the mixture and was kept under constant stirring for 24 h. After centrifugation, the product was washed with anhydrous dichloromethane and distilled water and dried in vacuum. The reaction pathway is shown in Scheme 2.

Scheme 2 Chemical modification of MWCNT

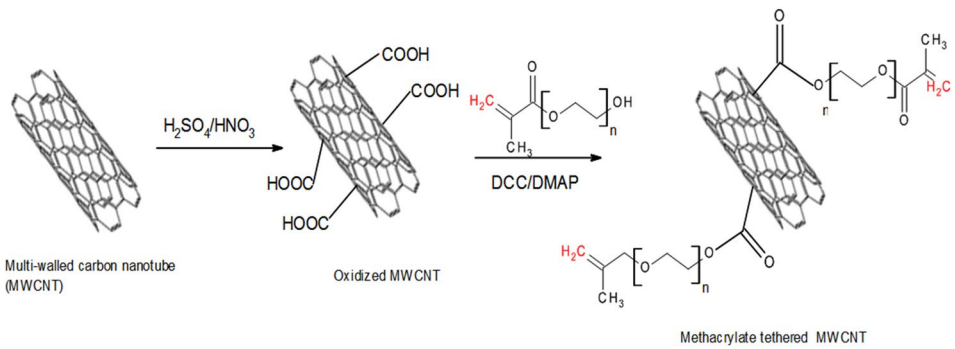

2.4 Preparation of sol–gel (SG)

The sol–gel precursor was prepared using the mixture of TEOS and MPTMS employed sol–gel conditions. 5 g of (0.024 mol) TEOS and 5.96 g of (0.024 mol) MPTMS were added into 1.73 mL (0.096 mol) distilled water and 2.84 mL (0.098 mol) of ethanol solution. Then, *p*-toluenesulfonic acid (p-TSA) as a catalyst (0.062 g; 3.6×10^{-4} mol) was added by slow addition and stirred continuously at room temperature for 12 h to obtain a sol–gel precursor.

2.5 Preparation of Hybrid Materials

UV curable formulations were prepared by mixing the calculated amounts of epoxy acrylate LR 8992 and poly(dimethyl siloxane-urethane methacrylate) as reactive oligomers, HDDA and nonbornyl acrylate as crosslinkers, *N*-vinyl pyrrolidone (NVP) as reactive diluent, PEGMA functionalized MWCNTs, sol–gel precursor and hydrophobic nanosilica. As an example P2 composition contains; 1.4 g of LR8992, 1.4 g of PDMS-U methacrylate, 0.4 g of NVP, 2 g of MWCNTs, 0.4 g of HDDA, 0.4 g of norbornyl acrylate and 0.08 g Irgacure 184. The composition of all composite films is also listed in Table 1. Each formulation was prepared in a beaker with adequate stirring. After mixing to homogenization, the beaker content heated to 40 °C was kept under vacuum for 3 min to remove dissolved gases during mixing. The UV-curable films were prepared onto Teflon mold (10 mm × 950 mm × 1 mm) and cured under UV irradiation (OSRAM, 300 W, 12 mW/cm^2) for 3 min. The films were annealed around at 100 °C for 24 h to achieve high degree cross-linking via condensation of silanol groups. An illustration of the UV-cured hybrid material along with the structures of the monomers used in this work can be seen in Scheme 3.

Table 1 Recipe for the formulations of the composites

	LR8992 (g)	PDMS-U methacrylate (g)	NVP (g)	MWCNTs (wt%)	Sol–gel (wt%)	Hydrophobic nanosilica (wt%)
P2	1.4	1.4	0.4	2	–	–
P2-5SG	1.4	1.4	0.4	2	5	–
P2-10SG	1.4	1.4	0.4	2	10	–
P2-2NS	1.4	1.4	0.4	2	–	2
P2-5NS	1.4	1.4	0.4	2	–	5
P4	1.4	1.4	0.4	4	–	–
P4-5SG	1.4	1.4	0.4	4	5	–
P4-5NS	1.4	1.4	0.4	4	–	5

All formulations containing 10 wt% HDDA, 10 wt% Norbornyl acrylate, and 2 wt% and Irgacure-184

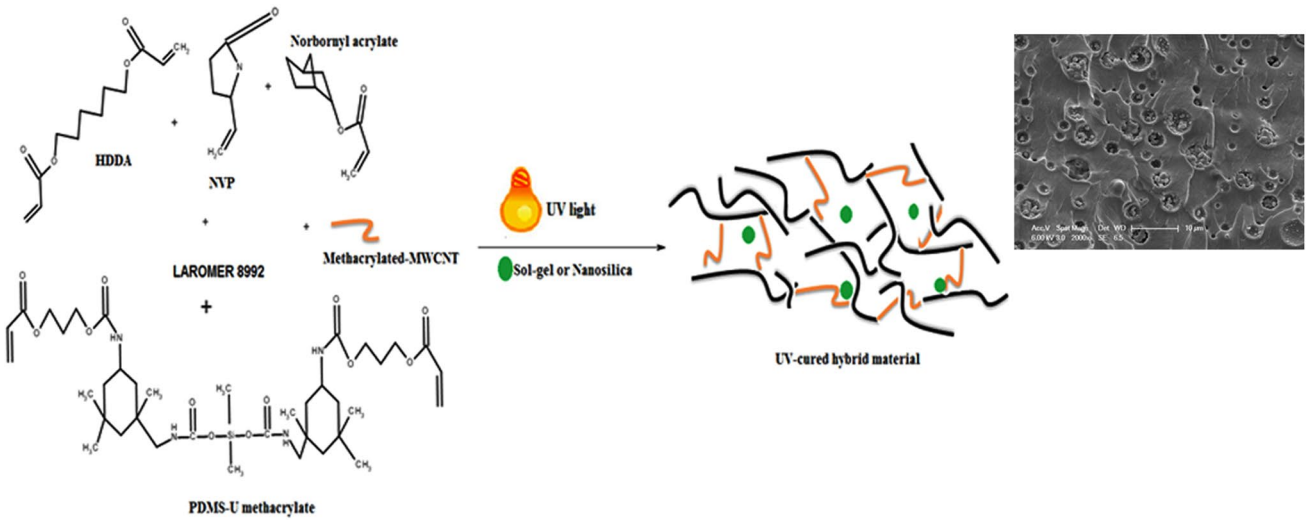

Scheme 3 Preparation of MWCNT, sol–gel and nanosilica containing hybrid material

2.6 Characterization

The morphology of composite films was analyzed on a Philips XL30 ESEM-FEG/EDAX microscope. The films were prepared by freeze fracturing in liquid nitrogen, and a gold coating of approximately 300 Å was applied.

Fourier transform infrared (FTIR) spectroscopy was performed on a Perkin Elmer attenuated total reflectance-FTIR spectrophotometer. All FTIR spectra were collected at the range from 4000 to 400 cm^{-1}.

Thermal analysis of the films was performed via a Perkin–Elmer Thermogravimetric Analyzer Pyris 1 TGA model. The films were run from 30 to 750 °C with a heating rate 10 °C/min under air atmosphere.

Mechanical properties of the composite films were investigated. Stress–strain tests were carried out using a Zwick Z010 universal tensile tester with a crosshead speed of 3 mm/min at room temperature. The measurements represent the average of at least five runs.

The wettability characteristics of the coatings were determined on a Kruss (Easy Drop DSA-2) tensiometer. The contact angles were measured by means of sessile drop test method in which drops were created by using a syringe. Measurements were made using 3–5 µl drops of distilled water. For each sample, at least five measurements were made, and the average was taken.

3 Results and Discussion

3.1 Structural Characterization

FT-IR spectrum was used for determinate to the functional groups attached to carbon nanotube. Figure 1 shows the FTIR spectra of PEGMA, carboxylated MWCNT, and PEGMA functionalized MWCNT, respectively. In curve a, the wide band around 3342 cm^{-1} O–H stretching vibration and the band of C=O group at 1727 cm^{-1} were observed. The strong absorption at 2927 and 2854 cm^{-1} correspond to methylene groups of PEGMA. The peak of 1099 cm^{-1} was the characteristic C–O stretching of PEGMA [22, 23]. In curve b, the band at 1711 cm^{-1} associated with carboxylic groups because of the oxidation of some carbon atoms on the surface of the MWNTs by nitric acid. The strong and broad band at 3200–2345 cm^{-1} can be related to the O–H stretch from strongly hydrogen-bonded –COOH. The peaks at 1650 and 3725 cm^{-1} can be associated with carboxylate anion stretching of the carboxylated MWCNT and free hydroxyl groups, respectively [24]. In curve c, the band at 1721 cm^{-1} related to C=O stretching of PEGMA became less intense in the PEGMA functionalized CNT. Two more strong peaks appear at 2926 and 2850 cm^{-1} because of the C–H stretching in the PEG chain. Furthermore, the PEGMA functionalized

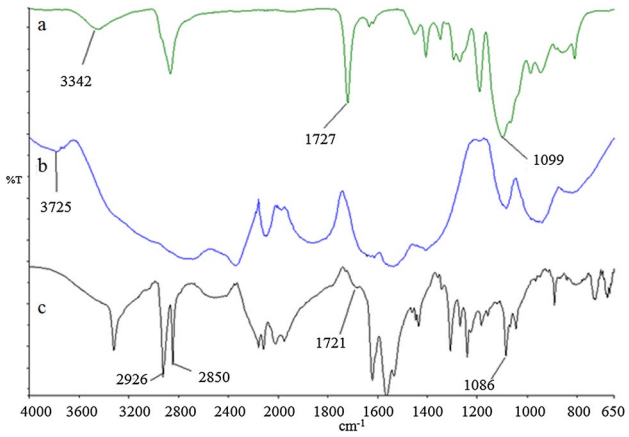

Fig. 1 FTIR spectra of (*a*) PEGMA, (*b*) oxidized MWCNT, and (*c*) PEGMA functionalized MWCNT, respectively

MWCNT spectrum shows a peak at 1086 cm^{-1} related to the C–O stretching of the ether group [25]. These peaks indicate that CNT covalently functionalized with linear PEGMA.

TGA was used to investigate the degree of functionalization of MWCNTs with PEGMA. The TGA and DTG spectra of MWCNT and PEGMA-functionalized MWCNT are shown in Fig. 2. As shown in Fig. 2, pure CNT showed one step weight loss in the temperature range from 600 to 800 °C. On the other hand, PEGMA-MWCNT showed weight loss in the temperature range from 200 to 320 °C due to decomposition of the PEG chains. In addition, the weight loss in the temperature range from 600 to 800 °C corresponds to the degradation of CNTs. DTG curves shows the inflection points for these decompositions (Fig. 2b).

The characterization of synthesized PDMS based urethane methacrylate was identified by ATR–FTIR and ^{1}H-NMR spectroscopy techniques. In the first step, the seconder NCO groups of IPDI were reacted with HEMA [26, 27]. However, as well as IPDI with one HEMA derivative (Scheme 1a), a mixture of IPDI with two HEMA derivatives (Scheme1b) and IPDI with no HEMA derivatives may occur. The intermediate-product mostly contains monoacrylated IPDI, since the two-NCO groups in IPDI differ in their reactivity due to the difference in the point of location of –NCO groups. It is reported that secondary NCO is more reactive than primary one in the presence of DBTDL catalyst. The higher reactivity of the secondary isocyanate is probably due to a larger electronic density on the isocyanate function, as observed by other authors [26]. This feature offers the possibilities for synthesizing controlled polyurethane structures.

Figure 3a illustrates the IR spectra of PDMS-U methacrylate. Since no purification is undertaken after first step, in the second step, a mixture of acrylates PDMS-U (mainly), diacrylated HEMA (seldom) can be obtained. However, the peaks at 1020 (Si–O vibration) and 795 cm^{-1} (Si–CH_3

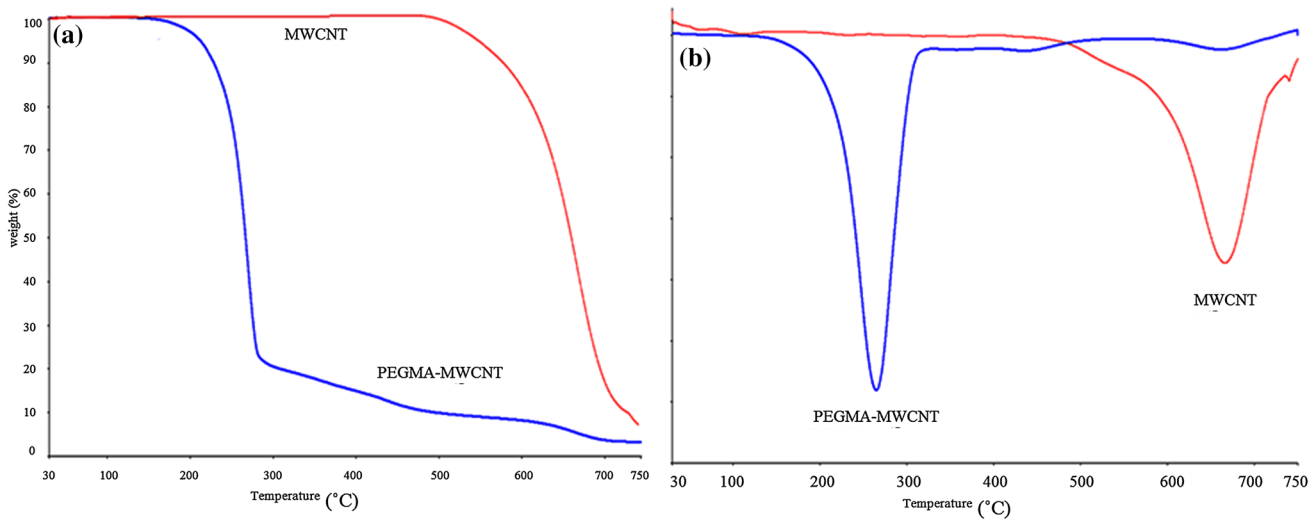

Fig. 2 TGA (**a**) and DTG (**b**) curves of the MWCNT and PEGMA-MWCNT

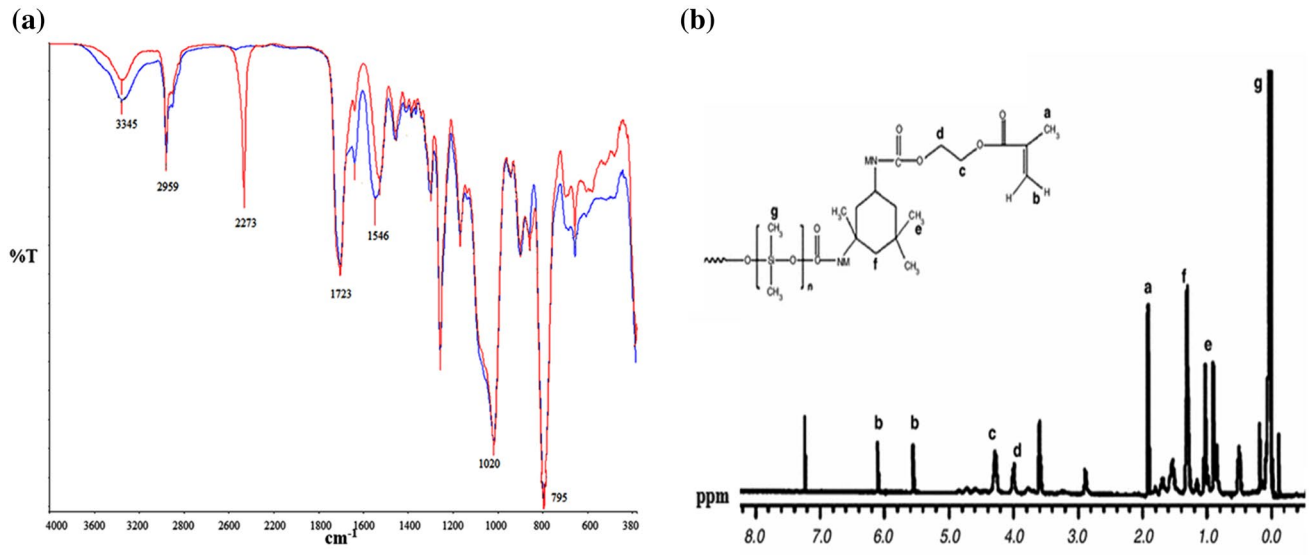

Fig. 3 FTIR and ^{1}H-NMR spectra of the PDMS urethane methacrylate

rocking) indicating that siloxane groups have been introduced into the polyurethane chains successfully. Moreover the absorption peaks at 3345 cm^{-1} (N–H stretching), 1723 cm^{-1} (C=O stretching) and 1546 cm^{-1} (N–H vibration) are typical peaks for polyurethane [28]. Additionally, the characteristic absorption of the NCO groups at 2273 cm^{-1} disappeared. The majority of the NCO groups of IPDI was reacted with hydroxyl groups of PDMS. However, very small amount of NCO groups may also have reacted with alcohol or water that may be present in the environment. The ^{1}H-NMR spectrum of PDMS-U methacrylate showed in Fig. 3b. The peaks from 0.96 to 2.9 ppm are due to methyl (CH_3) and methylene (CH_2) protons of PDMS-U methacrylate. Hydrogen of NHCO group is observed at 3.7 ppm. The –CH_3 group of PDMS is observed at 0.14 ppm. The peaks at 4.0 and 4.3 ppm are related to methylene protons of HEMA. The characteristic acrylate protons and CH_3 groups of HEMA were observed at 5.5–6.1 and 1.93 ppm, respectively.

3.2 Morphology of the Composite Films and Functionalized MWCNT

The surface morphology of the functionalized MWCNT was studied using SEM. Figure 4 shows the SEM micrograph for MWCNT, COOH-MWCNT and PEGMA functionalized

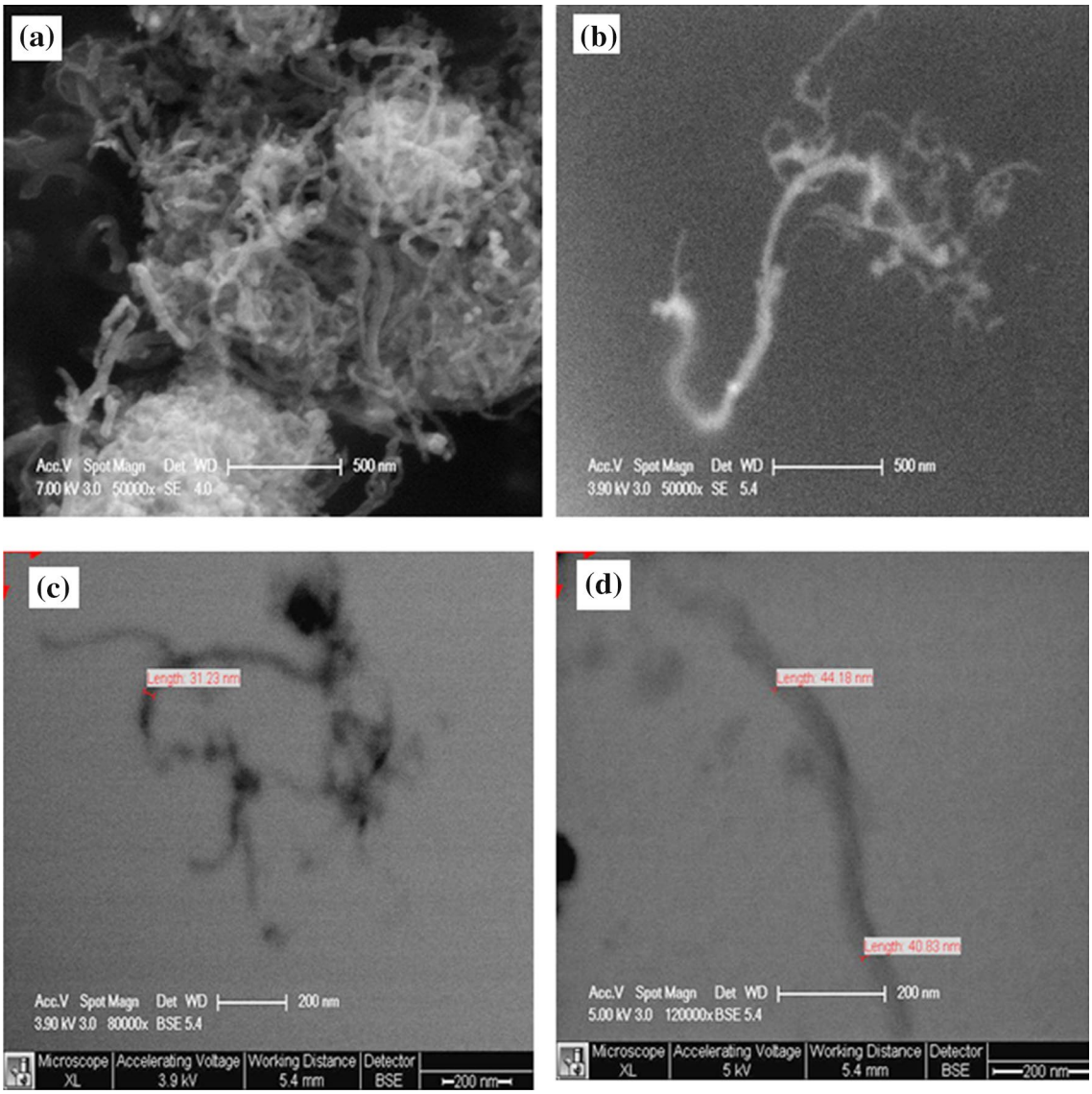

Fig. 4 SEM micrograph of **a** MWCNT, **b, c** COOH-MWCNT and **d** PEGMA functionalized MWCNT

MWCNT, respectively. It is clear from the Fig. 4a that the MWCNTs consist of tangled tubes [29]. Yudianti et al. [30] reported that the acid treatment creates nanodefects on nanotube walls. Liu et al. also reported acid (a mixture of H_2SO_4/HNO_3) treatment cut the highly tangled long MWCNTs into shorter. Thus, open-ended tubes containing many carboxylic groups are produced [31]. In the present work, the acid treatment was applied to the MWCNTs. The SEM images of COOH-MWCNTs are shown in Fig. 4b, c. It is clearly seen that after acid treatment the length of the MWCNTs became shorter that of its original size (Fig. 4b). In addition, it could be noticed that the diameter of the MWCNTs upon functionalization with PEGMA increased slightly (Fig. 4d).

The morphology of the composite films was also investigated by SEM. In Fig. 5, the fractured surface of P2, P2-5SG, P2-10SG, P2-5NS and P4-5SG composite films are presented. The SEM image of P2 exhibits the spherical domains. This phase separated morphology may be attributed to micro-micellization of aliphatic polyester acrylate based hydrophilic PU and hydrophobic PDMS based PU chains. In Fig. 5a, it was seen that, PEGMA modified CNTs particles mainly accumulated in these spherical regions. Moreover, SiO_2 nanoparticles obtained by sol–gel reaction demonstrated agglomeration in the spherical domains of the polymer matrix (Fig. 5a–c). To overcome the phase separated silica agglomeration hydrophobic silica was used as a reinforcer. In Fig. 5a–f, it can be observed that hydrophobic nanosilica homogenously dispersed throughout the polymer matrix and showed good compatibility with hydrophobic polymer.

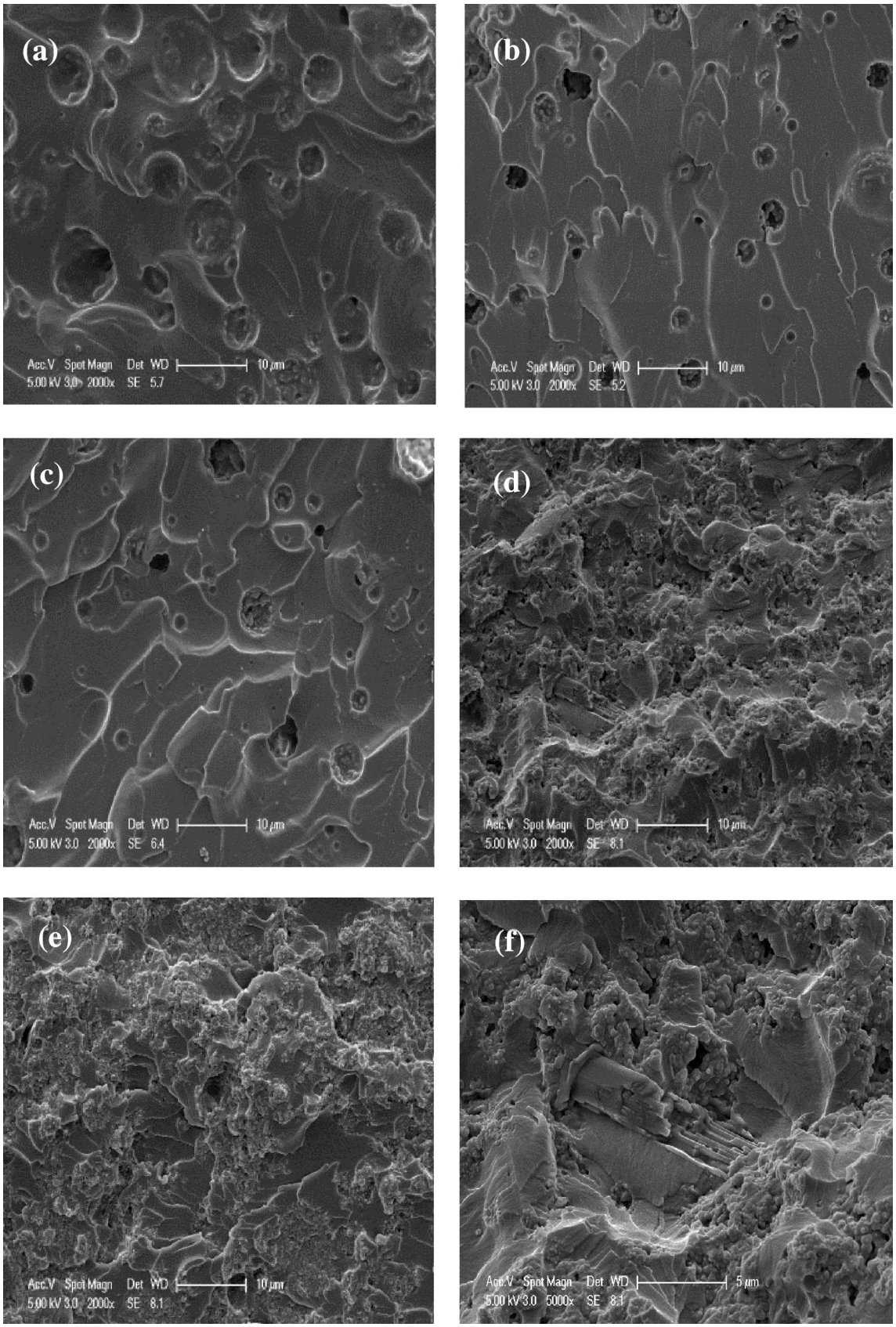

Fig. 5 SEM images of composites containing different fillers, **a** P2, **b** P2-5SG, **c** P2-10SG, **d** P2-2NS, **e** P2-5NS, **f** P4-5NS

The sol–gel particles have spherical morphology and diameter of particles is under 1 µm as can be seen Fig. 6. Hydrophilic sol–gel particles located within the spherical region mainly composed of epoxy acrylate resin (LR 8992) since sol–gel is highly immiscible with PDMS. Whereas hydrophobic nano-silica particles are highly compatible with PDMS-U methacrylate resin. Therefore homogeneous dispersion was achieved (Fig. 5e).

3.3 Thermogravimetric Analysis

Thermal properties of the composite films were investigated via thermal gravimetric analysis and the results are listed in Table 2. Temperature scan was performed from 30 to 750 °C under air atmosphere. The thermal degradation curves of the films with different weight percentages of MWCNT, sol–gel (SG) and hydrophobic NS are presented in Fig. 7. Corresponding derivative curves are also presented in these figures.

It can be seen from the results that all formulations exhibited similar two-step degradation profiles TGA curves indicated that water and organic solvents successfully removed from the composite films because there is no weight loss below 100 °C. The two weight loss ranges of all composite films are showed in Table 2.

For P2 sample, two weight loss peaks are observed; the first weight loss temperature (T1) was found as 212 °C corresponds to the weight loss of organic groups attached onto the surface of the MWCNTs [32]. While T1 was found as 213 °C for P2-5SG, it was determined as 269, 259 and 271 °C for P2-10SG, P2-2NS and P2-5NS, respectively. The

Table 2 Thermal properties of the composite films

	T1 (°C)	T2 (°C)	Char at 750 °C
P2	212	394	0.33
P2-5SG	213	397	2.20
P2-10SG	269	398	3.64
P2-2NS	259	406	3.21
P2-5NS	271	412	4.77
P4	259	413	0.53
P4-5SG	231	414	2.88
P4-5NS	267	414	5.25

results revealed that the addition of sol–gel and hydrophobic nanosilica has a significant contribution to the thermal stability of the films at low temperatures. The maximum weight loss temperature (T2) was found as 394 °C due to the beginning of polymer network degradation. The improvement in the degradation temperatures may be due to the strong interaction of functionalized carbon nanotube and nanosilica with polymer backbone. Sample P2-5NS observed the highest thermal stability compare to P2-5SG, P2-10SG and P2-2NS.

While the increasing of MWCNTs ratio (from 2 to 4%) similar degradation profile was experienced at higher decomposition temperatures. The effect of CNT–CNT and polymer–CNT interactions is the most likely cause the increase in thermal stability. This improved thermal stability is due to the known protective effect of the MWCNTs against thermal decomposition of the composites [33]. Char yields were also found to increase in the series parallel to

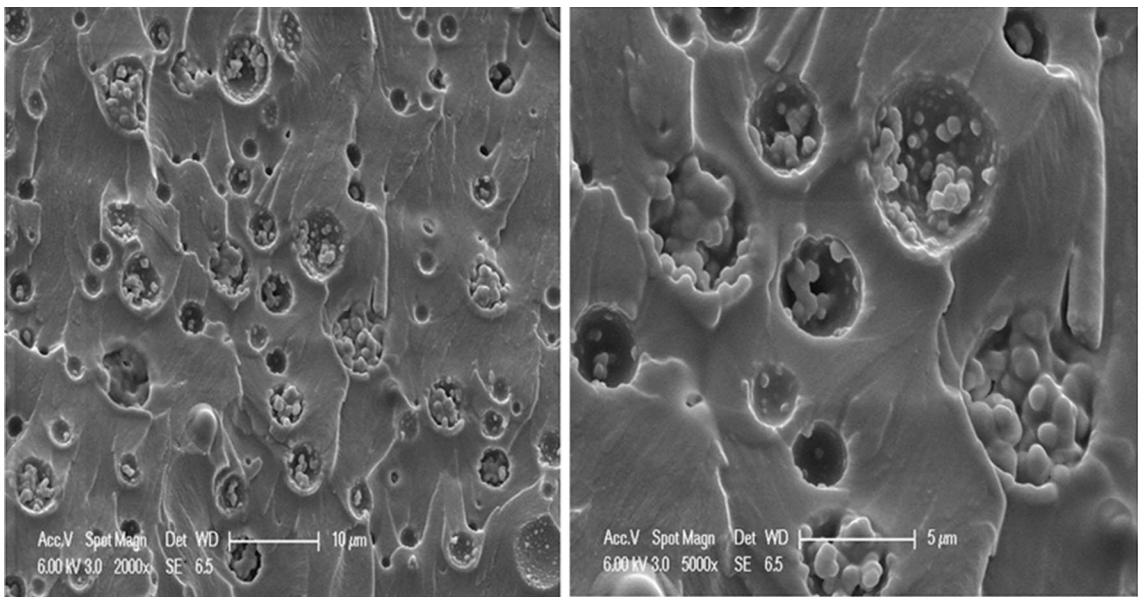

Fig. 6 SEM images of sol–gel in polymeric matrix

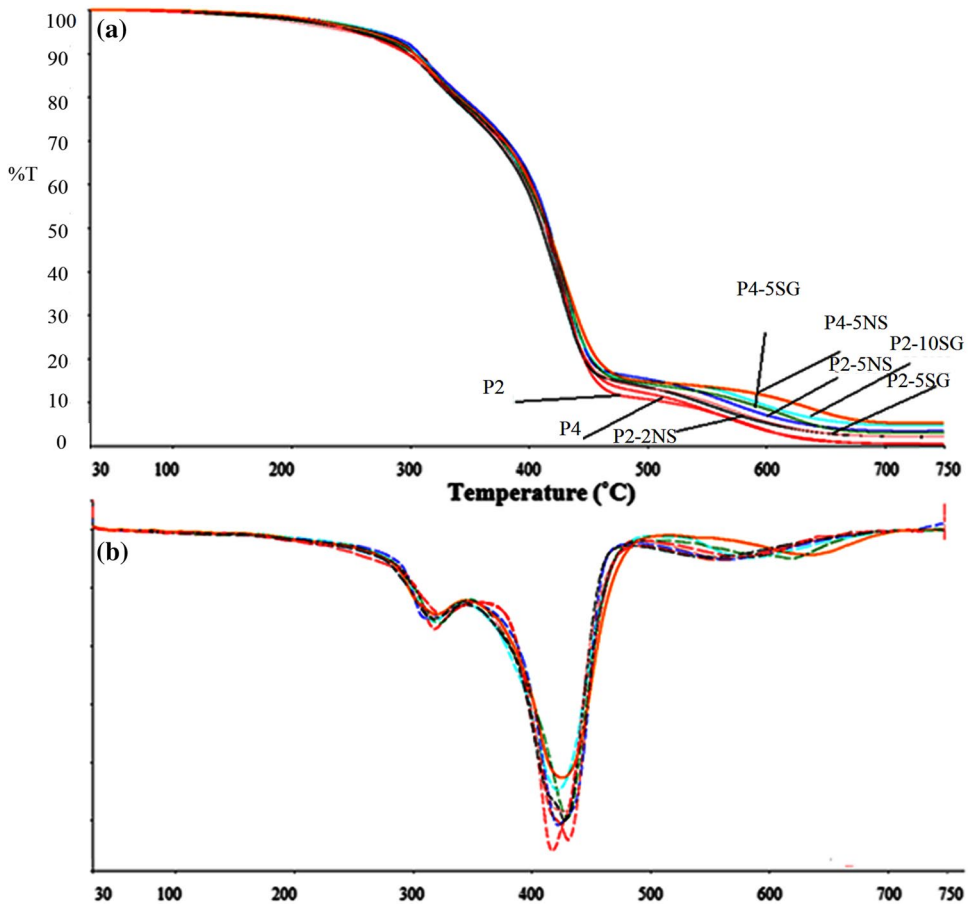

Fig. 7 TGA (**a**) and DTG (**b**) curves of the nanocomposite films under air atmospheres

the increase in the silica and nanosilica content. The char content of P2 sample was 0.33%. With increasing of carbon nanotube the char content of P4 increased to 0.53%. Sol–gel (from 5 to 10) and nanosilica (from 2 to 5) addition to P2 increased the char yield by 1.44 and 1.56%, respectively. Moreover, the char yield increased with increasing amount of MWCNTs from 0.33 to 0.53%.

3.4 Mechanical Properties

As can be seen from Table 3, sol–gel and nano-silica containing samples P2-5SG, P2-10SG, P2-2NS and P2-5NS exhibit an increase in the values of modulus and tensile strength. The modulus and tensile strength of all samples were higher than P2. The sample containing 5 wt% sol–gel, P2-5SG had a 250 MPa modulus and 136 MPa tensile strength. In the P2 series, P2-5NS has a maximum value of modulus (302 MPa) and tensile strength (299 MPa). In the P4 series, the 5 wt% nanosilica containing sample (P4-5NS) showed higher modulus and tensile strength than its 5 wt% sol–gel (P4-5SG).

The high content, size and aggregation of silica particles would lead to stress concentrations on the silica/polymer interface. As can be seen from Fig. 6b the regular distribution of sol–gel domains through the composite matrix, improved the mechanical strength and the modulus and tensile strength was increased. However, to overcome the phase separated morphology, the addition of hydrophobic silica instead of sol–gel was attempted. Nanoparticle aggregation causes defects within composite films due to its layering [34]. It is not possible to achieve an efficient stress transfer if the particles are not well-dispersed [35]. In this study, since low amount of hydrophobic nanosilica was incorporated in to the

Table 3 Mechanical properties and contact angle values of the composite films

	Modulus (MPa)	Tensile strength (MPa)	Elongation (%)	Contact angle
P2	245	144	35	67 ± 0.3
P2-5SG	250	136	23	75 ± 1.2
P2-10SG	304	171	13	85 ± 2.0
P2-2NS	257	187	26	86 ± 1.8
P2-5NS	302	299	18	88 ± 4.0
P4	199	148	11	78 ± 0.76
P4-5SG	238	141	11	81 ± 1.8
P4-5NS	315	209	12	89 ± 2.2

composites, the agglomeration was prevented and enhanced modulus and tensile strength values were achieved.

3.5 Wettability of the Composite Films

The surface wettability properties of the films were identified using water contact angle measurements. As it can be seen from the Table 3, the contact angle value P2 was found as 67°. When 5% sol–gel was added to the formulation (P2), the contact angle increased to 75°. The hydrophobicity of the composites increased in the presence of sol–gel. The contact angle of P2-10SG was 85°. The nanosilica particles containing series were showed a gradual increase. Contact angle values in 4% MWCNT containing series increased gradually and were found as 78°, 81° and 89° for P4, P4-5SG, P4-5NS, respectively.

4 Conclusions

In this study, the PEGMA functionalized MWCNTs containing PDMS-PU methacrylate based UV curable nanocomposite films were prepared and the effect of the sol–gel precursor and the hydrophobic nanosilica on the characteristic properties were studied. MWCNTs were first treated by a mixture of NHO_3 and H_2SO_4 and then PEGMA grafting on the surface to form a UV-curable functional groups. Methacrylate modified MWCNTs were covalently bonded to polymer matrix. As expected, sol–gel silica and hydrophobic nanosilica containing composite films demonstrated the high decomposition temperature because of the inorganic Si–O–Si network. Furthermore, the incorporation of MWCNTs effectively improved the thermal stability due to the protective effect of CNTs. The morphological studies indicated that modified MWCNTs and hydrophobic nanosilica nanoparticles showed homogeneous dispersion in the PU methacrylate matrix and exhibited better performance with respect to sol–gel type silica reinforcement.

Acknowledgements This work was supported by Marmara University, Commission of Scientific Research Project (M.U.BAPKO) under Grant FEN-C-YLP-191212-0355.

References

1. J. Han, in *Carbon Nanotubes: Science and Applications*, ed. by M. Meyyappan (CRC Press LLC, Boca Raton, FL, 2004), p. 99
2. E.T. Thostenson, Z.F. Ren, T.W. Chou, Compos. Sci. Technol. **61**, 1899 (2001)
3. P.C. Ma, N.A. Siddiqui, G. Marom, J.K. Kim, Compos. Part A **41**, 1345 (2010)
4. X.S. Wang, Q.Q. Li, J. Xie, Z. Jin, J.Y. Wang, Y. Li, K.L. Jiang, S.S. Fan, Nano Lett. **9**, 3137 (2009)
5. P. Liu, Eur. Polym. J. **41**, 2693 (2005)
6. J. Safari, Z. Zargenar, J. Saudi Chem. Soc. **18**, 85 (2014)
7. K. Esumi, M. Ishigami, A. Nakajima, K. Sawada, H. Honda, Carbon **34**, 279 (1996)
8. P.C. Ma, J.K. Kim, in *Carbon Nanotubes for Polymer Reinforcement*, 1st edn ed. by R. Rafiee (CRC Press, Boca Raton, FL, 2011)
9. S. Banerjee, T. Hemraj-Benny, S.S. Wong, Adv. Mater. **17**, 17 (2005)
10. F. Haghighat, M. Mokhtary, J. Inorg. Organomet. Polym. Mater. **27**, 779 (2017)
11. J.N. Coleman, U. Khan, Y.K. Gun'ko, Adv. Mater. **18**, 689 (2006)
12. J.N. Coleman, U. Khan, W.J. Blau, Y.K. Gun'ko, Carbon **44**, 1624 (2006)
13. T. Fujigaya, S. Haraguchi, T. Fukumaru, N. Nakashima, Adv. Mater. **20**, 2151 (2008)
14. W. Zhou, J. Xu, W. Shi, Thin Solid Films **516**, 4076 (2008)
15. A. Eitan, K. Jiang, D. Dukes, R. Andrews, L.S. Schadler, Chem. Mater. **15**, 3198 (2003)
16. X.D. Zhao, X.H. Fan, X.F. Chen, C.P. Chai, Q.F. Zhou, J. Polym. Sci. A **44**, 4656 (2006)
17. C. Kingston, R. Zepp, A. Andrady, D. Boverhof, R. Fehir, D. Hawkins, J. Roberts, P. Sayre, B. Shelton, Y. Sultan, V. Vejins, W. Wohlleben, Carbon **68**, 33 (2004)
18. Bayer MaterialScience, Additives Polym. **2010**, 4 (2010)
19. T. Liu, S. Guo, in *Properties of Polyurethane/Carbon Nanotube Nanocomposites*. Polymer Nanotube Nanocomposites: Synthesis, Properties and Applications (Scrivener, Salem, MA, 2010) pp. 141–176
20. H. Xia, M. Song, Soft Matter **1**, 386 (2005)
21. B. Oktay, N. Kayaman-Apohan, J. Coat. Technol. Res. **10**, 785 (2013)
22. H. Liu, M. Liu, L. Zhang, L. Ma, J. Chen, Y. Wang, React. Funct. Polym. **70**, 294 (2010)
23. D. Zheng, Y.Y. An, S. Yang, W. Wu, W. Xu, G. Liu, C. Yang, Y. Dan, Z. Xu, S. Wu, Int. J. Polym. Mater. **63**, 115 (2013)
24. M.A. Atieh, O.Y. Bakather, B. Al-Tawbini, A.A. Bukhari, F.A. Abuilaiwi, M.B. Fettouhi, Bioinorg. Chem. Appl. **2010**, 603978 (2010)
25. E. Pramono, S.B. Utomo, V. Wulandari, F. Clegg, in *Journal of Physics: Conference Series*, vol. 776 (IOP Publishing, Bristol, 2016),p. 012053
26. S. Villeneuve, M. Lavıolette, M. Auger, S. DeSılets, J. Polym. Sci. Part C **35**, 2991 (1997)
27. H.K. Ono, F.N. Jones, S.P. Pappas, J. Polym. Sci. **23**, 509 (1985)
28. B. Oktay, R.D. Toker, N. Kayaman-Apohan, Polym. Bull. **72**, 2831 (2015)
29. M.A. Salam, R. Burk, Arab. J. Chem. **10**, S921 (2017)
30. R. Yudianti, H. Onggo, Sudirman, Y. Saito, T. Iwata, J. Azuma, Open Mater. Sci. J. **5**, 242 (2011)
31. J. Liu, A.G. Rinzler, H. Dai, J.H. Hafner, R.K. Bradley, P.J. Boul, Science, **280** 1253 (1993)
32. V.T. Le, C.L. Ngo, Q.T. Le, T.T. Ngo, D.N. Nguyen, M.T. Vu, Adv. Nat. Sci. **4**, 035017 (2013)
33. A. Rostami, M. Masoomi, M.J. Fayazi, M. Vahdati, RSC Adv. **5**, 32880 (2015)
34. S. Karatas, N. Kayaman-Apohan, H. Demirer, A. Güngör, Polym. Adv. Technol. **18**, 490 (2007)
35. J. Liu, Y. Gao, F. Wang, M. Wu, J. Appl. Polym. Sci. **75**, 384 (2000)